Reactions of the HO$_2$ Radical with CH$_3$CHO and CH$_3$C(O)O$_2$ in the Gas Phase

Alexandre Tomas, Eric Villenave, and Robert Lesclaux*

Laboratoire de Physico-Chimie Moléculaire, UMR 5803 CNRS, Université Bordeaux I, 33405 Talence Cedex, France

Flash photolysis UV absorption techniques were used to study the HO$_2$ + CH$_3$C(O)O$_2$ reaction. It was found that the reaction HO$_2$ + CH$_3$CHO ⇌ CH$_3$CH(OH)O$_2$ (2, −2) can interfere with the kinetic measurements. Thus, the kinetics and thermochemistry of this reaction were investigated. The UV spectrum of the CH$_3$CH(OH)O$_2$ radical was determined, and the rate constant for the association reaction was measured to be k_2 = 4.4 × 10^{-14} cm^3 molecule^{-1} s^{-1} at 298 K, with an uncertainty factor of about 2. The reaction was found to be equilibrated near room temperature, and the equilibrium constant was determined between 298 and 373 K: $K_2 = k_2/k_{-2}$ = 1.9 × 10$^{-(27\pm1)}$ exp[+(6925 ± 840 K)/T] cm^3 molecule^{-1}. This corresponds to ΔH°_{298} = −64 ± 8 kJ mol^{-1} and ΔS°_{298} = −157 ± 6 J K^{-1} mol^{-1} (errors are 2σ), the latter value being in good agreement with the calculated value, using the AM1 semiempirical method. The kinetics of the reactions CH$_3$C(O)O$_2$ + HO$_2$ → CH$_3$C(O)OOH + O$_2$ (1a) and CH$_3$C(O)O$_2$ + HO$_2$ → CH$_3$C(O)OH + O$_3$ (1b) were determined in the temperature range 273−403 K, using low acetaldehyde concentrations, so that reaction 2 could be neglected. The initial radical concentrations were measured carefully and were consistent with the concentrations of the precursors (acetaldehyde and methanol). The rate expression is k_1 = (6.4 ± 2.5) × 10^{-13} exp[+(925 ± 120 K)/T] cm^3 molecule^{-1} s^{-1}, yielding k_1 = (1.42 ± 0.07) × 10^{-11} cm^3 molecule^{-1} s^{-1} at 298 K. The quoted errors are 2σ, and the global uncertainty is estimated at 15%. The branching ratio of channel 1b, $\beta_1 = k_{1b}/k_1$, was determined by measuring the residual absorption, from 230 to 280 nm, at sufficiently long time, so that all radicals had recombined. It was verified that the UV spectrum of the residual absorption was the same as that of ozone, within uncertainty. The resulting value β_1 = 0.20 ± 0.02 was derived, independent of temperature over the range studied.

Introduction

Acetylperoxy radicals play a major role in the atmospheric degradation of organic compounds. They undergo fast reactions with other peroxy radicals and with nitrogen oxides, either propagating the chain reactions forming ozone or acting in efficient termination reactions. In addition, in polluted atmospheres, the association reaction with NO$_2$ forms the well-known peroxyacetylnitrate CH$_3$C(O)O$_2$NO$_2$ (PAN). Due to its relatively high stability, contrasting with that of other peroxynitrates, PAN is able to transport nitrogen oxides long away from sources.[1] In less polluted atmospheres, the reactions with other peroxy radicals, HO$_2$ or RO$_2$, become critical toward the environmental impact of CH$_3$C(O)O$_2$, as NO$_x$ levels may be low.

Several studies on the reactivity of the acetylperoxy radical have been performed these past years, using different techniques, and the kinetics of the CH$_3$C(O)O$_2$ reactions are now well-established. In contrast, the kinetics of the reaction of CH$_3$C(O)O$_2$ with HO$_2$ radicals is still a matter of some controversy, as the two principal investigations on the rate constant of this reaction by Moortgat et al.[2] and Crawford et al.[3] differ by a factor of nearly 3. Although the very recent recommendation of Tyndall et al.[4] was based essentially on the data reported by Moortgat et al.,[2] further work was obviously needed to understand the mechanism and the kinetics of this reaction.

The mechanism of the reaction of CH$_3$C(O)O$_2$ with HO$_2$ radicals proceeds via the following two molecular channels:

$$CH_3C(O)O_2 + HO_2 \rightarrow CH_3C(O)OOH + O_2 \quad (1a)$$
$$\rightarrow CH_3C(O)OH + O_3 \quad (1b)$$

The rate constant of reaction 1 was first determined by Moortgat et al.[2] in the temperature range 253−368 K, using the flash photolysis technique coupled to UV absorption spectrometry for real time radical monitoring. They proposed an Arrhenius expression of k_1 = 4.3 × 10^{-13} exp(+(1040 K)/T) cm^3 molecule^{-1} s^{-1}, giving k_1 = 1.3 × 10^{-11} cm^3 molecule^{-1} s^{-1} at 298 K. The branching ratio $\beta_1 = k_{1b}/k_1$ was found to be independent of temperature in the range investigated and equal to 0.33. The three end-product studies available to date for reaction 1,[3,5,6] reported smaller values for the branching ratio; i.e. β_1 = 0.25 (Niki et al.),[5] 0.27 (Horie et Moortgat),[6] and 0.12 (Crawford et al.)[3] at 298 K. Concerning the kinetics, a new investigation of reaction 1 was recently reported by Crawford et al.[3] using laser flash photolysis technique coupled with two different detection methods: time-resolved UV spectroscopy and transient IR absorption. They obtained a value of k_1 = 3.9 × 10^{-13} exp(+(1350 K)/T) cm^3 molecule^{-1} s^{-1} (269 K < T < 363 K), giving k_1 = 3.6 × 10^{-11} cm^3 molecule^{-1} s^{-1} at 298 K. Thus, the rate constant value at room temperature is approximately 3 times larger than the value reported by Moortgat et al.,[2] recommended in the last reviews on peroxy radicals.,[7−9]

* To whom correspondence should be addressed. E-mail: lesclaux@cribx1.u-bordeaux.fr.

Crawford et al.[3] attributed this difference to the occurrence of the reaction between HO_2 and CH_3CHO, forming the α-hydroxyperoxy radical $CH_3CH(OH)O_2$. This reaction was not taken into account by Moortgat et al.[2]

We report here the results of a reinvestigation of the kinetics of the $CH_3C(O)O_2 + HO_2$ reaction, using the flash photolysis technique coupled to UV absorption spectrometry. In a first part, we have investigated the reaction between HO_2 and CH_3CHO. As for the $HO_2 + HCHO$ reaction,[10] the reaction of HO_2 with CH_3CHO reveals an equilibrium, which was already mentioned by Roehl et al.:[11]

$$HO_2 + CH_3CHO + M \rightleftharpoons CH_3CH(OH)O_2 + M \quad (2,-2)$$

The equilibrium constant was determined in the 298−373 K temperature range and the corresponding thermochemical parameters were derived from these values by using the Second and Third Law thermodynamic analyses. In the latter case, the entropy change of reaction 2 was calculated using semiempirical calculations (AM1 level).

In a second part, the kinetics of the $CH_3C(O)O_2 + HO_2$ reaction were investigated between 273 and 403 K. The results obtained from the investigation of reaction 2 allowed us to set the experimental conditions under which the reaction of HO_2 with CH_3CHO did not occur to a significant extent, thus preventing any interference with kinetic measurements of reaction 1. In addition, much care was taken in this study to control accurately the initial concentrations of the HO_2 and $CH_3C(O)O_2$ radicals. The results are discussed and compared to previous data.

Experimental Section

A conventional flash photolysis technique coupled with absorption spectrometry in the ultraviolet spectral range was used for monitoring peroxy radical absorptions. With the experimental setup being described in detail in a previous work,[12] only the main features are described here.

The reaction cell consists of a Pyrex cylinder of 70 cm length and 4 cm diameter, which can be heated or cooled, depending on the desired temperature, the temperature being controlled within ±2 K. The continuous flow of the gas mixture was photolyzed by an argon flash lamp. The analyzing beam from a deuterium lamp passes once through the cell and is dispersed in a monochromator (2 nm resolution). The signal from the photomultiplier detector is sent to a digital oscilloscope and then transferred to a personal computer for averaging and analysis. Scattered light from the flash prevented all data from being recorded for approximately 50−100 μs after the flash. About 20−30 absorption time profiles were accumulated in order to reach a satisfactory signal-to-noise ratio. The total gas flow was adjusted so that the cell was completely replenished between two flashes, and, therefore, the photolysis of any reaction product was avoided.

Two distinct methods of generating radicals were used: the flash photolysis of Cl_2 in the presence of acetaldehyde and methanol for studying the kinetics of the reactions of HO_2 with CH_3CHO and with $CH_3C(O)O_2$ and the direct photolysis of CH_3-CHO for investigating the equilibrium of reactions 2 and −2.

1. Photolysis of Cl_2 in $CH_3CHO/CH_3OH/O_2/N_2$ Mixtures.
The photolysis of Cl_2 in the presence of CH_3CHO and CH_3OH yields $CH_3C(O)O_2$ and HO_2 radicals instantaneously on the time scale of the radical decay. The first steps of the reaction mechanism are the fast reactions 3−7, followed by the recombination reactions of peroxy radicals.
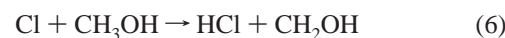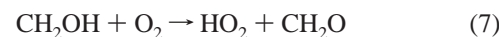
$$Cl_2 + h\nu(\lambda > 290 \text{ nm}) \rightarrow Cl + Cl \quad (3)$$

$$Cl + CH_3CHO \rightarrow HCl + CH_3CO \quad (4)$$
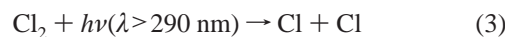
$k_4 = 7.2 \times 10^{-11}$ cm³ molecule⁻¹ s⁻¹ at 298 K [13]

$$CH_3CO + O_2 + M \rightarrow CH_3C(O)O_2 + M \quad (5)$$

$k_5 = 3.2 \times 10^{-12}$ cm³ molecule⁻¹ s⁻¹ at 298 K and 1 atm total pressure[13]

$$Cl + CH_3OH \rightarrow HCl + CH_2OH \quad (6)$$

$k_6 = 5.5 \times 10^{-11}$ cm³ molecule⁻¹ s⁻¹ at 298 K [13]

$$CH_2OH + O_2 \rightarrow HO_2 + CH_2O \quad (7)$$

$k_7 = 9.6 \times 10^{-12}$ cm³ molecule⁻¹ s⁻¹ at 298 K [13]

Typical concentrations (molecule cm⁻³) of reactants are as follows: $[CH_3CHO] = (0.05-3.3) \times 10^{16}$; $[CH_3OH] = (0.1-9.1) \times 10^{16}$; $[N_2] = (0.07-4.6) \times 10^{18}$; $[O_2] = (2.0-2.4) \times 10^{19}$; $[Cl_2] = (1.2-2.6) \times 10^{16}$, resulting in total peroxy radical concentrations of $(3-10) \times 10^{13}$ molecule cm⁻³. Note that the formation of radicals by direct photodissociation of precursors was avoided by using low concentrations of CH_3CHO and CH_3-OH and with radiations filtered by the Pyrex cutoff.

During all experiments, liquid reactants (CH_3CHO and CH_3-OH) were maintained at fixed temperatures (217 K for CH_3-CHO and 273 K for CH_3OH) and used in bubblers by passing nitrogen flow through the liquid. Their concentrations were controlled by mass flow controllers, which were calibrated before experiments. The chlorine concentration was controlled by UV absorption at 330 nm ($\sigma_{Cl_2} = 2.55 \times 10^{-19}$ cm² molecule⁻¹).[14]

2. Direct Photolysis of CH_3CHO in Oxygen. The equilibrium of the $CH_3CHO + HO_2$ reaction was investigated by flash photolysis experiments of $CH_3CHO/O_2/N_2$ gas mixtures, using high concentrations of CH_3CHO, typically $(0.3-1) \times 10^{18}$ molecule cm⁻³, completed with oxygen up to 760 Torr. Acetaldehyde was used by bubbling nitrogen ($[N_2] = (0.7-2.2) \times 10^{18}$ molecule cm⁻³) through the liquid maintained at 273 K. The concentration of CH_3CHO was controlled by both mass flow controllers and UV absorption at 310 nm ($\sigma_{CH_3CHO} = 2.93 \times 10^{-20}$ cm² molecule⁻¹).[13] The photolysis of CH_3CHO is expected to mainly proceed (>98%) via a single channel for radiations larger than 290 nm [13]

$$CH_3CHO + h\nu(\lambda > 290 \text{ nm}) \rightarrow CH_3 + HCO \quad (8)$$
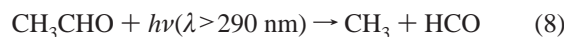
followed by the fast reactions

$$CH_3 + O_2 + M \rightarrow CH_3O_2 + M \quad (9)$$

$k_9 = 9.5 \times 10^{-13}$ cm³ molecule⁻¹ s⁻¹ at 298 K and 1 atm total pressure[13]

$$HCO + O_2 \rightarrow HO_2 + CO \quad (10)$$
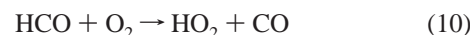
$k_{10} = 5.2 \times 10^{-12}$ cm³ molecule⁻¹ s⁻¹ at 298 K [13] leading to equal proportions of CH_3O_2 and HO_2 radicals.

All reagents CH_3CHO (Aldrich, 99.5%), CH_3OH (Aldrich, 99.95%), Cl_2 (Messer, 5% in N_2, purity > 99.9%), O_2 (Messer,
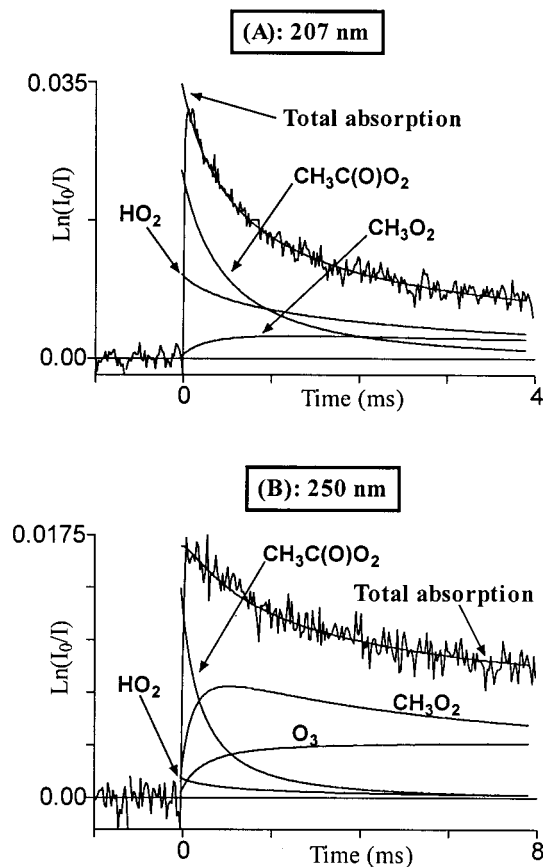
Figure 1. Typical plots obtained in the case of the photolysis of Cl$_2$/CH$_3$CHO/CH$_3$OH/O$_2$/N$_2$ mixtures: (A) 207 and (B) 250 nm. Solid lines represent simulations.

purity > 99.995%), and N$_2$ (AGA Gaz spéciaux, purity > 99.995%) were used without further purification.

Results

1. Kinetics and Thermochemistry of the HO$_2$ + CH$_3$CHO Reaction.

$$HO_2 + CH_3CHO + M \rightleftharpoons CH_3CH(OH)O_2 + M \quad (2, -2)$$

The necessity of investigating this reaction occurred when studying the kinetics of reaction 1 and carefully monitoring the initial concentrations of both CH$_3$C(O)O$_2$ and HO$_2$ radicals. The occurrence of reaction 2 was characterized through flash photolysis experiments of Cl$_2$ in the presence of CH$_3$CHO and CH$_3$OH in O$_2$/N$_2$ mixtures, by varying the CH$_3$CHO concentration by a factor of about 70. It should be emphasized that, considering that the rate constant ratio $k_4/k_6 = 1.35 \pm 0.05$ is now well-established,[13,15,16] initial concentrations of CH$_3$C(O)-O$_2$ and HO$_2$ radicals can be anticipated by accurately controlling the concentration of precursors:

$$\frac{[CH_3C(O)O_2]_{ini}}{[HO_2]_{ini}} = \frac{k_4[CH_3CHO]}{k_6[CH_3OH]}$$

Decay traces of total peroxy radical absorptions were monitored at two different wavelengths, i.e. 207 and 250 nm. Typical decay traces are shown in Figure 1. At 207 nm, both CH$_3$C(O)O$_2$ and HO$_2$ radicals absorb significantly, with respective cross-section values of 6.80×10^{-18} and 4.10×10^{-18} cm^2 molecule^{-1}.[4] In contrast, the absorption cross-section of HO$_2$ is much smaller at 250 nm, where only the acetylperoxy radical

absorbs significantly: $\sigma(HO_2) = 4.6 \times 10^{-19}$ and $\sigma(CH_3C(O)-O_2) = 3.2 \times 10^{-18}$ cm^2 molecule^{-1}. Therefore, by comparison of initial absorptions at 207 nm and at 250 nm, we could verify the consistency between the precursor concentration ratio and the obtained initial radical concentration ratio.

An accurate determination of the observed [CH$_3$C(O)O$_2$]$_{ini}$/[HO$_2$]$_{ini}$ initial concentration ratio can be performed by simulation of decay traces, taking the complete reaction mechanism into account, as detailed in Table 1. The differential equation system relative to concentrations was resolved by using the Runge−Kutta integration method at the fourth order. Simulations allowed us to extrapolate the absorption signal to time zero for an accurate determination of the initial peroxy radical concentrations, which were then compared to the predicted concentration ratio.

In a first approach, we assumed that the reaction of HO$_2$ with acetaldehyde was negligible, by reference to a previous estimation of the rate constant k_2 ($\approx 1 \times 10^{-15}$ cm^3 molecule^{-1} s^{-1}).[17] We observed that for low CH$_3$CHO concentrations, below about 5×10^{15} molecule cm^{-3}, the [CH$_3$C(O)O$_2$]$_{ini}$/[HO$_2$]$_{ini}$ concentration ratio obtained from simulations at 207 and 250 nm corresponded to that expected. However, at higher concentrations, the apparent radical concentration ratio increased with increasing [CH$_3$CHO] and keeping [CH$_3$CHO]/[CH$_3$OH] constant. This behavior is illustrated in Figure 2A,B, where decay traces are compared to the simulations performed with the expected concentration ratios.

In a second approach, we included the reaction of HO$_2$ with acetaldehyde in the reaction mechanism with a rate constant value of 5×10^{-14} cm^3 molecule^{-1} s^{-1}, referring to the recent value of Crawford et al.[3] The subsequent reactions of the CH$_3$-CH(OH)O$_2$ radical formed in reaction 2 were also included. These additional reactions are listed in Table 2 with the corresponding rate constants, which were adjusted in this work and found very close to the corresponding reactions of the CH$_2$-(OH)O$_2$ radical.[10,18] In such conditions, all experimental traces could be correctly simulated, using the UV absorption cross-sections of the CH$_3$CH(OH)O$_2$ radical determined in this work (see below).

The rate constant k_2 was adjusted by fitting the decay traces obtained at 207 and 250 nm and for CH$_3$CHO concentrations included in the $(1-4) \times 10^{16}$ molecule cm^{-3} range. The rate constant k_{-2} value of the reverse reaction had only a small influence on the determination of k_2 at room temperature, but, nevertheless, it was taken into account in data analyses. The resulting values of k_2 were fairly scattered (from 2×10^{-14} to 9×10^{-14} cm^3 molecule^{-1} s^{-1}; see Table 3), but, nevertheless, a reliable average value could be obtained from 12 determinations:

$$k_2 = (4.4 \pm 1.4) \times 10^{-14} \text{ cm}^3 \text{ molecule}^{-1} \text{ s}^{-1} \text{ at}$$
$$298 \text{ K and } P = 1 \text{ atm O}_2$$

This value is in good agreement with that estimated by Crawford et al.[3], $k = 5.0 \times 10^{-14}$ cm^3 molecule^{-1} s^{-1} at 298 K. By analogy with the reaction of HO$_2$ with HCHO,[10] we have assumed that k_2 does not exhibit any significant temperature dependence.

The uncertainty quoted above in the expression of k_2 represents 2σ, resulting from the data obtained at various wavelengths, principally 207 and 250 nm. Systematic uncertainties come mainly from the rate constant of the reverse reaction −2 (50%) and from the absorption cross-sections of the CH$_3$-CH(OH)O$_2$ radical (50%). Combining both statistical and

TABLE 1: Chemical Mechanism Used in Simulations in the Case of Cl$_2$ Photolysis Experiments

no.	reaction		rate constant[a]	ref
1a	CH$_3$C(O)O$_2$ + HO$_2$	→ CH$_3$C(O)OOH + O$_2$	$k_1 = 6.4 \times 10^{-13}$ exp((925 K)/T)	this work
1b		→ CH$_3$C(O)OH + O$_3$	$k_{1b}/k_1 = 0.20$	this work
11	CH$_3$C(O)O$_2$ + CH$_3$C(O)O$_2$	→ 2CH$_3$C(O)O + O$_2$	$k_{11} = 2.5 \times 10^{-12}$ exp((500 K)/T)	4
12	CH$_3$C(O)O + M	→ CH$_3$ + CO$_2$ + M	assumed instantaneous	
9	CH$_3$ + O$_2$ + M	→ CH$_3$O$_2$ + M	assumed instantaneous	
13	HO$_2$ + HO$_2$ + M	→ H$_2$O$_2$ + M	$k_{13} = 1.7 \times 10^{-33}$[M] exp((1000 K)/$T$) $+ 2.3 \times 10^{-13}$ exp((600 K)/T)	14
14a	CH$_3$C(O)O$_2$ + CH$_3$O$_2$	→ CH$_3$C(O)O + CH$_3$O + O$_2$	$k_{14a} = 1.85 \times 10^{-12}$ exp((500 K)/T)	4
14b		→ CH$_3$C(O)OH + CH$_2$O + O$_2$	$k_{14b} = 2.0 \times 10^{-13}$ exp((500 K)/T)	4
15	CH$_3$O + O$_2$	→ CH$_2$O + HO$_2$	assumed instantaneous	
16	HO$_2$ + CH$_3$O$_2$	→ CH$_3$OOH + O$_2$	$k_{16} = 4.1 \times 10^{-13}$ exp((750 K)/T)	4
17a	CH$_3$O$_2$ + CH$_3$O$_2$	→ 2CH$_3$O + O$_2$	$k_{17a} = 5.1 \times 10^{-13}$ exp((424 K)/T)	4
17b		→ CH$_3$OH + CH$_2$O + O$_2$	$k_{17b} = 1.9 \times 10^{-14}$ exp((706 K)/T)	4

[a] Unit: k, cm^3 molecule^{-1} s^{-1}. [M] is the total molecular concentration.
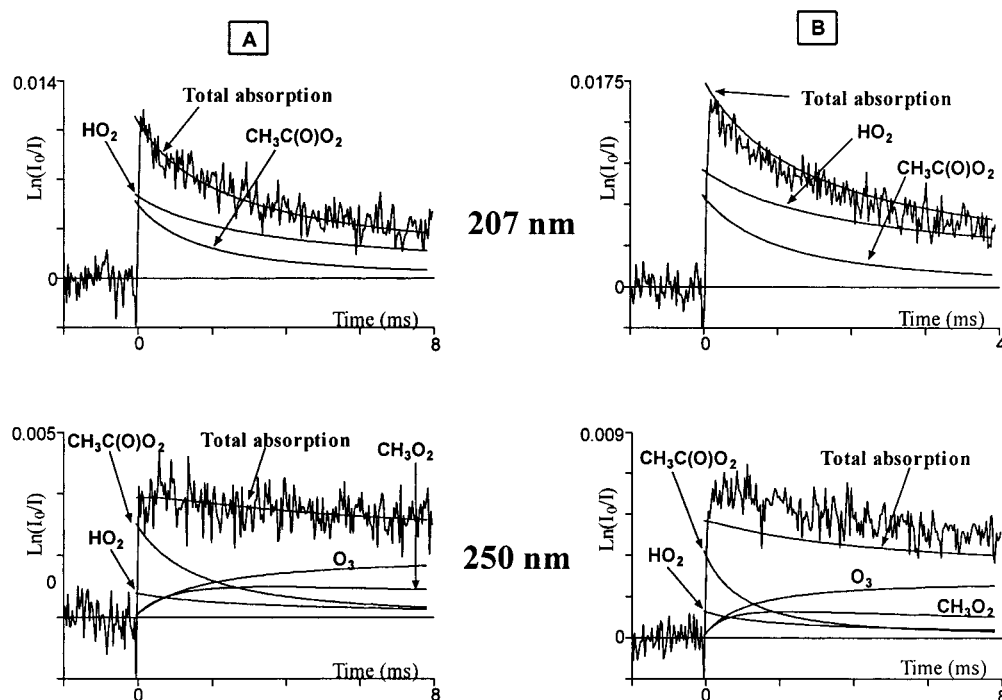
Figure 2. Decay traces at 207 and 250 nm obtained in the case of the photolysis of Cl$_2$/CH$_3$CHO/CH$_3$OH/O$_2$/N$_2$ mixtures: (A) [CH$_3$CHO] = 8.1 × 10^{14} and (B) [CH$_3$CHO] = 3.2 × 10^{16} molecule cm^{-3}. In both cases, [CH$_3$CHO]/[CH$_3$OH] = 0.4. Solid lines represent simulations.

TABLE 2: Reactions Added to the Chemical Mechanism in Table 1 To Account for the HO$_2$ + CH$_3$CHO Reaction in Simulations

no.	reaction		rate constant[a]	ref
2	CH$_3$CHO + HO$_2$ + M	→ CH$_3$CH(OH)O2 + M	$k_2 = 4.4 \times 10^{-14}$ (P = 1 atm of O$_2$)[b]	this work
−2	CH$_3$CH(OH)O$_2$ + M	→ CH$_3$CHO + HO$_2$ + M	$k_2 = 2.3 \times 10^{13}$ exp((6925 K)/T) (P = 1 atm)	this work
18a	CH$_3$C(O)O$_2$ + CH$_3$CH(OH)O$_2$	→ CH$_3$C(O)O + CH$_3$CH(OH)O + O$_2$	$k_{18} = 1.0 \times 10^{-11}$	22
18b		→ 2CH$_3$C(O)OH + O$_2$	$k_{18a}/k_{18} = 0.95$	c
19a	CH$_3$CH(OH)O$_2$ + CH$_3$CH(OH)O$_2$	→ 2CH$_3$CH(OH)O + O$_2$	$k_{19} = 6 \times 10^{-12}$	d
19b		→ CH$_3$CH(OH)OH + CH$_3$C(O)OH + O$_2$	$k_{19a}/k_{19} = 0.9$	d
20	CH$_3$CH(OH)O$_2$ + HO$_2$	→ CH$_3$CH(OH)OOH + O$_2$	$k_{20} = 1.2 \times 10^{-11}$	d
21	CH$_3$CH(OH)O + O$_2$	→ CH$_3$C(O)OH + HO$_2$	$k_{21} = 3.5 \times 10^{-14}$	d
22a	CH$_3$CH(OH)O$_2$ + CH$_3$O$_2$	→ CH$_3$CH(OH)O + CH$_3$O + O$_2$	$k_{22} = 3 \times 10^{-12}$	23
22b		→ molecular products	$k_{22a}/k_{22} = 0.60$	c

[a] Units: k, cm^3 molecule^{-1} s^{-1}; except k_{-2}, s^{-1}. [b] Assumed independent of temperature by analogy with the corresponding reaction of HO$_2$ with HCHO.[10] [c] Arithmetic mean of the branching ratios of the corresponding self-reactions. [d] Corresponds to the measurement of Veyret et al.[10] and Burrows et al.[18] for the CH$_2$(OH)O$_2$ radical.

systematic uncertainties, we estimate a global uncertainty factor of about 2 on the rate constant k_2.

Determination of the UV Absorption Cross-Sections of the CH$_3$CH(OH)O$_2$ Radical. The second set of experiments consisted of direct photolysis of CH$_3$CHO in the presence of excess

oxygen and using higher acetaldehyde concentrations than previously, (3−10) × 10^{17} molecule cm^{-3}. The acetaldehyde concentration was monitored accurately by UV absorption at 310 nm. Under such conditions, both initial absorptions and kinetics of decay traces obtained at 207 and 250 nm could not

TABLE 3: Rate Constants Values Obtained at 298 K for the Reaction HO$_2$ + CH$_3$CHO

wavelength (nm)	[CH$_3$CHO] (molecule cm^{-3})	[CH$_3$OH] (molecule cm^{-3})	k_2 (cm^3 molecule^{-1} s^{-1})
250	3.2×10^{16}	3.2×10^{16}	4.8×10^{-14}
250	3.2×10^{16}	6.4×10^{16}	4.5×10^{-14}
250	1.6×10^{16}	1.6×10^{16}	6.5×10^{-14}
250	1.6×10^{16}	1.6×10^{16}	2.8×10^{-14}
250	3.2×10^{16}	4.7×10^{16}	6.2×10^{-14}
250	1.6×10^{16}	2.3×10^{16}	9.2×10^{-14}
250	3.2×10^{16}	3.2×10^{16}	3.4×10^{-14}
230	3.2×10^{16}	6.4×10^{16}	5.0×10^{-14}
207	3.2×10^{16}	4.7×10^{16}	3.4×10^{-14}
207	3.2×10^{16}	3.2×10^{16}	2.9×10^{-14}
207	1.6×10^{16}	1.6×10^{16}	2.5×10^{-14}
207	3.2×10^{16}	3.2×10^{16}	1.85×10^{-14}
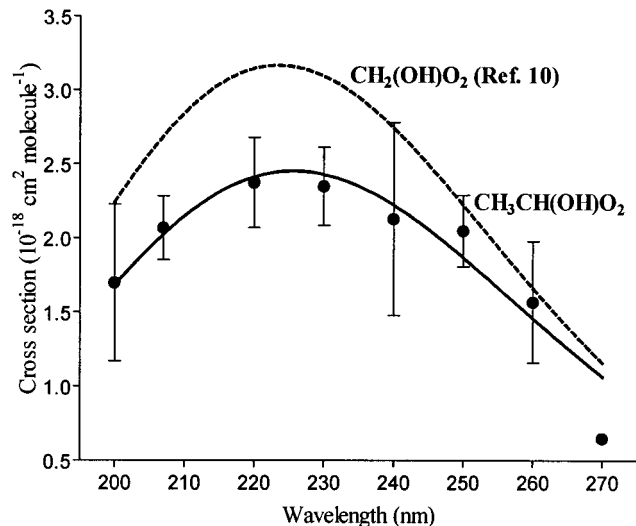
Figure 3. UV absorption spectrum of the CH$_3$CH(OH)O$_2$ radical. The dashed line represents the UV spectrum of the CH$_2$(OH)O$_2$ radical, from ref 10, which has been corrected according to recent cross-section recommendations in ref 4. Error bars represents 2σ.

be reproduced correctly if the reaction of HO$_2$ with CH$_3$CHO was not taken into account.

Considering both the high concentrations of CH$_3$CHO and the value of k_2 obtained in the first set of experiments, HO$_2$ radicals formed by reaction 10 were instantaneously converted into CH$_3$CH(OH)O$_2$ radicals through reaction 2, compared to the time scale of the radical decay. In addition, at 298 K, the equilibrated reaction 2 was completely shifted toward the CH$_3$-CH(OH)O$_2$ formation, according to the equilibrium constant determined below. In contrast, at temperatures higher than around 400 K, decay traces could be simulated by only taking the CH$_3$O$_2$ and HO$_2$ radicals into account in the reaction mechanism. In other words, we estimated that the contribution of CH$_3$CH(OH)O$_2$ radicals to the initial absorption could be neglected at temperatures higher than 400 K. The UV spectrum of the CH$_3$CH(OH)O$_2$ radical was derived from pairs of experiments performed at both 298 and 423 K, with $6.5 \cdot 10^{17}$ to $8.1 \cdot 10^{17}$ molecule cm^{-3} of acetaldehyde. Simulations of traces recorded at 423 K allowed us to determine the absolute concentration of radicals produced by the flash, by essentially referring to the HO$_2$ absorption. Then decay traces recorded at 298 K under the same conditions, were fitted by adjusting the CH$_3$CH(OH)O$_2$ radical cross-section and the UV spectrum was obtained by repeating similar experiments at different wavelengths, from 200 to 270 nm. The resulting UV spectrum is shown in Figure 3, together with that of CH$_2$(OH)O$_2$ for comparison,[10] and the corresponding cross-sections are listed in Table 4. Note that this procedure is equivalent to determine

TABLE 4: Absorption Cross-Section Values of the CH$_3$CH(OH)O$_2$ Radical

wavelength (nm)	measured cross-sections (cm^2 molecule^{-1})	fitted cross-sections[a] (cm^2 molecule^{-1})
200	$(1.70 \pm 0.53) \times 10^{-18}$	1.68×10^{-18}
207	$(2.07 \pm 0.21) \times 10^{-18}$	2.02×10^{-18}
210		2.15×10^{-18}
220	$(2.38 \pm 0.30) \times 10^{-18}$	2.41×10^{-18}
230	$(2.35 \pm 0.26) \times 10^{-18}$	2.43×10^{-18}
240	$(2.13 \pm 0.65) \times 10^{-18}$	2.22×10^{-18}
250	$(2.05 \pm 0.24) \times 10^{-18}$	1.87×10^{-18}
260	$(1.57 \pm 0.41) \times 10^{-18}$	1.46×10^{-18}
270	0.65×10^{-18}	1.07×10^{-18}

[a] Using the expression $\sigma/(10^{-18}$ cm^2 molecule$^{-1}) = 2.45 \cdot \exp(-25.8[\ln(225.6/(\lambda/\text{nm}))]^2)$; corresponds to the solid line in Figure 3.

TABLE 5: Values of the Equilibrium Constant K_2 as a Function of Temperature

temp (K)	[CH$_3$CHO] (molecule cm^{-3})	k_2 (s^{-1})	K_2 (cm^3 molecule^{-1})
298	$(1.6-3.2) \times 10^{16}$	750 ± 350	$(5.9 \pm 4.5) \times 10^{-17}$
310	$(3.6-7.4) \times 10^{17}$	4200 ± 2000	$(1.0 \pm 0.7) \times 10^{-17}$
317	$(3.3-6.4) \times 10^{17}$	8500 ± 2500	$(5.2 \pm 3.0) \times 10^{-18}$
343	$(4.1-7.8) \times 10^{17}$	$(4.2 \pm 1.5) \times 10^4$	$(1.05 \pm 0.7) \times 10^{-18}$
363	$(2.1-7.8) \times 10^{17}$	$(1.1 \pm 0.3) \times 10^5$	$(4.0 \pm 2.3) \times 10^{-19}$
373	5.2×10^{17}	$(2.2 \pm 1.1) \times 10^5$	$(2.0 \pm 1.6) \times 10^{-19}$

the CH$_3$CH(OH)O$_2$ spectrum against that of HO$_2$, using the recently recommended HO$_2$ absorption cross-sections.[4]

Uncertainties on the cross-section values arise principally from those on the precursor concentration (15%) and on the HO$_2$ absorption cross-section (8%). Other sources of errors, such as those on the CH$_3$O$_2$ cross-sections and on the extrapolation of decay traces to time zero, represent only minor contributions ($\approx$5%). Taking the statistical uncertainty ($\approx$15%) into account, the overall uncertainty on σ(CH$_3$CH(OH)O$_2$) is estimated at 25%.

Determination of the Equilibrium Constant. The equilibrium constants K_2 of reaction 2 was determined at six temperatures (298, 310, 317, 343, 363, and 373 K) from the fit of decay traces at both 207 and 250 nm, using the absorption cross-sections of CH$_3$CH(OH)O$_2$ determined in this work. At 298 K, K_2 was determined by photolyzing Cl$_2$ in the presence of relatively low concentrations of acetaldehyde, $\approx$3 $\times$ 10^{16} molecule cm^{-3}, whereas at the other temperatures, acetaldehyde was photolyzed directly, using concentrations in the range of $(2.1-7.8) \times 10^{17}$ molecule cm^{-3}. Decay traces were simulated by adjusting k_{-2} and keeping k_2 constant. The resulting values of the equilibrium constants K_2 are listed in Table 5. A linear regression yields

$$K_2 = k_2/k_{-2} = 1.9 \times 10^{-(27\pm1)} \times$$
$$\exp[+(6925 \pm 840 \text{ K})/T] \text{ cm}^3 \text{ molecule}^{-1}$$

Thermodynamical parameters were derived from the van't Hoff plot of $\ln(K_2/\text{atm}^{-1})$ vs $1/T$ illustrated in Figure 4 and listed in Table 6. Thermodynamical parameters were also derived from the Third Law method of analysis, by calculating the entropy of formation of each species using semiempirical calculations (AM1).[19] The results, also included in Table 6, are in very good agreement with those obtained from the Second Law method of analysis, thereby demonstrating the consistency between experimental and theoretical approaches.

It is interesting to compare the thermodynamical parameters obtained for equilibrium 2 to those previously reported for the HCHO + HO$_2$ ⇌ CH$_2$(OH)O$_2$ equilibrium[10] (see Figure 4 and

TABLE 6: Experimental and Theoretical (AM1 Semiempirical Method) Thermodynamical Parameters[a] for the Reaction HO_2 + CH_3CHO (HCHO) $\rightleftharpoons$ $CH_3CH(OH)O_2$ ($HCH(OH)O_2$)

			Calculated Entropy Values		
molecules	HO_2	CH_3CHO	$CH_3CH(OH)O_2$	HCHO	$CH_2(OH)O_2$
$S°_{298}$ (J K^{-1} mol^{-1})	220.7	266.1	323.1	224.6	286.3

	Comparison between calculated and experimental parameters			
	$\Delta S°_{298,exp.}$	$\Delta H°_{298,\text{ second Law}}$	$\Delta S°_{298,theor.}$	$\Delta H°_{298,\text{ third Law}}$
CH_3CHO	-167	-67	-164	-66
HCHO	-146	-68	-159	-71

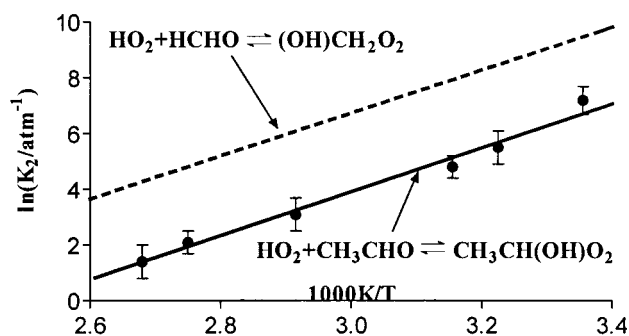[a] Units: ΔS, J K^{-1} mol^{-1}; ΔH, kJ mol^{-1}.

Figure 4. Van't Hoff plots ($\ln(K_2/\text{atm}^{-1})$ vs $1/T$) for the equilibrated reaction 2. The data for the reaction HO_2 + HCHO $\rightleftharpoons$ $CH_2(OH)O_2$ are from ref 10.

Table 6). It is satisfying to note that the parameters are quite similar for both reactions, even though the $CH_2(OH)O_2$ adduct is significantly more stable than the $CH_3CH(OH)O_2$ one. This consistency adds to the reliability of the data.

2. Kinetics of the $CH_3C(O)O_2$ + HO_2 Reaction.

$$CH_3C(O)O_2 + HO_2 \rightarrow CH_3C(O)OOH + O_2 \quad (1a)$$

$$\rightarrow CH_3C(O)OH + O_3 \quad (1b)$$
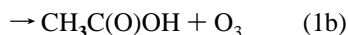
The kinetics of the $CH_3C(O)O_2$ + HO_2 reaction were investigated by photolysis of $Cl_2/CH_3CHO/CH_3OH/O_2/N_2$ mixtures. Analyzing carefully previous studies of this reaction,[2,3] it appears that the observed discrepancies likely arise from the initial radical concentrations which were not controlled with sufficient accuracy. In the work of Moortgat et al.,[2] the experimental conditions were not sufficiently well-described and the reaction of HO_2 with CH_3CHO was not taken into account. In the work of Crawford et al.,[3] the HO_2 + CH_3CHO reaction was taken into account, but not the reverse reaction and, according to their Table 2, there was a significant inconsistency between the observed ratios of radical concentrations and those

TABLE 7: Values of Absorption Cross-Sections[a] Used in the Simulations

	absorption cross-section		
absorbing species	$\lambda = 207$ nm	$\lambda = 250$ nm	ref
$CH_3C(O)O_2$	6.80×10^{-18}	3.22×10^{-18}	4
HO_2	4.10×10^{-18}	4.67×10^{-19}	4
CH_3O_2	1.86×10^{-18}	3.78×10^{-18}	4
$CH_3CH(OH)O_2$	2.07×10^{-18}	2.05×10^{-18}	this work
O_3	4.34×10^{-19}	1.08×10^{-17}	14
H_2O_2	3.80×10^{-19}	8.30×10^{-20}	14
CH_3OOH	4.00×10^{-19}	3.98×10^{-20}	14

[a] Unit: cm^2 molecule^{-1}.

expected from precursor concentrations. For those reasons, we have been very careful, in the present work, in controlling the initial radical concentration with accuracy. Sufficiently low concentrations of CH_3CHO (($0.5-1.6$) $\times 10^{15}$ molecule cm^{-3}) were used in order to prevent the reaction of HO_2 with CH_3CHO from occurring to a significant extent. In addition, it was verified for each run that the ratio $[CH_3C(O)O_2]_{ini}/[HO_2]_{ini}$ was always that expected from precursor concentrations. This was found to be true in all cases, within uncertainties, showing thereby that the contribution of the $CH_3CH(OH)O_2$ radical formed in the HO_2 + CH_3CHO reaction could be neglected. Nevertheless, this reaction was always included in the reaction mechanism used in analysis of experimental signals.

As experimental time profiles corresponded to the contributions of all absorbing species, it was necessary to deconvolute decay traces by numerical simulations, to determine the partial contributions of $CH_3C(O)O_2$ and HO_2 radical absorptions. The complete chemical mechanism (detailed in Tables 1 and 2) was taken into account. Simulations were performed using the most recent recommendations of absorption cross-sections, rate constants, and branching ratios related to the species and reactions involved in the system.[4] The values used for those parameters are given in Tables 1, 2, and 7. The only adjustable parameters were k_1 for the traces recorded over short time scales and the branching ratio $\beta_1 = k_{1b}/k_1$, forming ozone, for traces recorded over long time scales. Those parameters were optimized automatically, using nonlinear least-squares fitting. Note that all decay traces corresponding to the self-reaction of the $CH_3C(O)O_2$ radical (in the absence of CH_3OH) were correctly simulated with the recommended rate constant for k_{11}.[4]

Rate constants were measured at five temperatures between 273 and 403 K and the ratio $[CH_3C(O)O_2]_{ini}/[HO_2]_{ini}$ was varied from 0.3 to 3. For each run, a pair of traces was recorded at two wavelengths, 207 and 250 nm (Figure 1). The kinetic information resulted essentially from simulations of decay traces recorded at 207 nm, where $CH_3C(O)O_2$ and HO_2 have their principal absorption band. At 250 nm, the initial absorption corresponded almost exclusively to $CH_3C(O)O_2$, and thus, it was used for the determination of the $[CH_3C(O)O_2]_{ini}/[HO_2]_{ini}$

TABLE 8: Measured Values of the Rate Constants k_1

temp (K)	[CH$_3$CHO][a]	[CH$_3$OH][a]	[CH$_3$C(O)O$_2$]$_{ini}$[b]	[HO$_2$]$_{ini}$[b]	k_1[c]
273	0.53	1.2	1.9	3.5	1.87
273	0.53	1.2	2.05	3.5	1.70
273	0.53	2.4	1.6	4.0	1.60
273	0.88	1.2	2.8	2.6	2.01
273	1.2	1.2	2.3	2.8	2.03
273	1.2	1.2	3.2	2.3	1.75
273	1.8	1.2	3.4	2.1	1.98
average					1.85 ± 0.15
293	0.48	1.1	0.9	2.3	1.57
293	0.48	1.1	1.6	4.3	1.38
293	0.81	0.97	2.3	1.9	1.60
293	0.81	1.6	1.4	1.6	1.53
293	0.81	2.4	1.2	2.1	1.40
293	0.81	3.2	1.0	2.1	1.50
293	0.97	0.97	2.0	1.5	1.71
293	1.6	0.97	2.2	0.8	1.42
293	1.6	1.6	1.9	1.7	1.55
293	1.6	1.6	2.2	1.4	1.47
293	1.6	1.6	1.8	1.5	1.50
293	1.6	1.8	2.3	1.8	1.70
293	1.6	3.2	1.2	2.2	1.37
average					1.51 ± 0.07
343	0.42	0.98	1.6	3.0	0.871
343	0.42	0.98	2.0	3.5	1.01
343	0.42	2.0	1.3	3.9	0.864
343	0.70	0.98	2.5	2.5	0.988
343	0.98	0.98	2.6	2.0	1.03
343	1.4	0.98	2.8	1.6	1.02
average					0.96 ± 0.06
373	0.39	0.90	1.55	2.45	0.737
373	0.39	1.8	0.80	3.2	0.870
373	0.65	0.90	2.0	1.85	0.734
373	0.78	1.55	4.5	6.6	0.730
373	0.90	1.3	4.1	7.5	0.700
373	0.90	0.90	1.9	1.4	0.897
373	1.3	0.90	2.1	1.35	0.716
373	1.3	1.3	6.8	4.2	0.695
average					0.76 ± 0.06
403	0.36	0.84	1.3	2.7	0.654
403	0.36	1.7	0.85	3.1	0.659
403	0.60	0.84	1.6	2.3	0.644
403	0.84	0.84	2.3	1.8	0.490
403	1.2	0.84	2.55	1.6	0.570
average					0.60 ± 0.08

[a] Unit: 10^{15} molecule cm^{-3}. [b] Unit: 10^{13} molecule cm^{-3}. [c] Unit: 10^{-11} cm^3 molecule^{-1} s^{-1}.

ratio. As the reaction proceeds, CH$_3$C(O)O$_2$, CH$_3$O$_2$, and O$_3$ absorb at that wavelength and the fit of absorption profiles provided a good indication about the validity of the reaction mechanism used for simulations. At longer time ($\approx$500 ms), the residual absorption essentially corresponds to that of ozone.

All the values obtained for k_1 are reported in Table 8, along with the experimental conditions. The temperature dependence of k_1 is displayed in Figure 5 in the form of an Arrhenius plot. The corresponding expression is

$$k_1 = (6.4 \pm 2.5) \times 10^{-13} \exp[+(925 \pm 120 \text{ K})/T]$$
$$\text{cm}^3 \text{ molecule}^{-1} \text{ s}^{-1} \quad (273 \text{ K} < T < 403 \text{ K})$$

yielding $k_1 = (1.42 \pm 0.07) \times 10^{-11}$ cm^3 molecule^{-1} s^{-1} at 298 K (errors are 2σ).

Systematic uncertainties arise principally from those on CH$_3$C(O)O$_2$ and HO$_2$ radical cross-sections,[4] resulting in errors on initial radical concentrations of about 8%. Additional errors may arise from the extrapolation to time zero at 207 nm (5%) and, to a lesser extent, from the kinetics of the cross-reaction
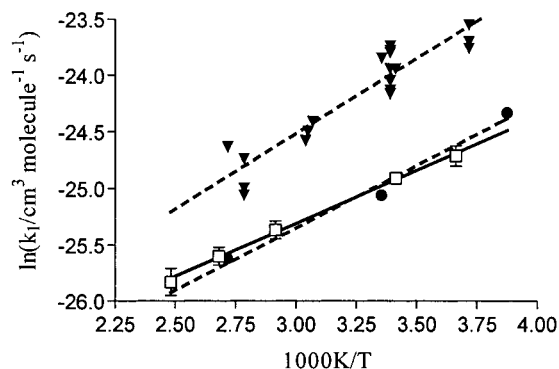

Figure 5. Arrhenius plot for the CH$_3$C(O)O$_2$ + HO$_2$ reaction rate constant. Triangles are from Crawford et al.,[3] circles from Moortgat et al.,[2] and open squares from this work.

(reaction 14) between CH$_3$C(O)O$_2$ and CH$_3$O$_2$ radicals (<5%). The resulting global uncertainty on k_1 is estimated at 15%, using the error propagation method.

The branching ratio $\beta_1 = k_{1b}/k_1$ was obtained from decay traces at 250 nm monitored over longer time scales (500 ms),
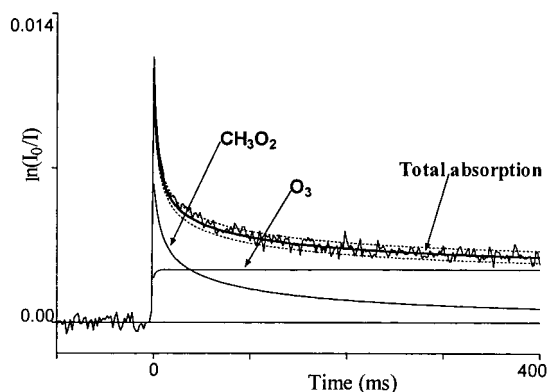
Figure 6. Decay trace obtained at 250 nm over long monitoring time in the case of $Cl_2/CH_3CHO/CH_3OH/O_2/N_2$ photolysis. The solid line represents the simulation using $\beta_1 = 0.20$. The upper and lower traces (dashed lines) represent the limits $\beta_1 = 0.22$ and 0.18.
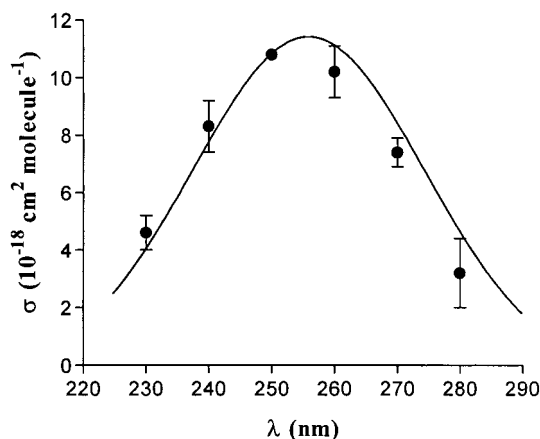

Figure 7. Comparison between the ozone UV absorption spectrum (solid line, ref 20) and the residual absorption spectrum observed when investigating the $HO_2 + CH_3C(O)O_2$ reaction kinetics (circles). The two spectra are scaled at 250 nm.

as illustrated in Figure 6. At such a long time, the residual absorption essentially corresponds to the ozone absorption $\sigma(250\text{ nm}) = 1.08 \times 10^{-17}$ cm^2 molecule^{-1},[20] since all radicals have recombined. Only small amounts of CH_3O_2 remained, which were easily taken into account by simulations. Experiments were performed at various wavelengths (from 230 to 280 nm) in order to verify that the spectrum of the residual absorption corresponded to that of ozone. This is illustrated in Figure 7. It is seen that the results are indistinguishable from the reference spectrum of ozone.[20] It should be emphasized that to determine accurately the initial radical concentrations, a pair of traces was recorded at 207 and 250 nm using a short time scale (5−10 ms) before recording a trace over long time (500 ms). The branching ratio derived from the average of 10 runs, gathered in Table 9, is $\beta_1 = k_{1b}/k_1 = 0.20 \pm 0.01$ at 298 K, where errors are 2σ. Propagation of systematic uncertainties associated predominantly with uncertainties in $\sigma(CH_3C(O)O_2)$ and $\sigma(HO_2)$ leads to a final value of $\beta_1 = 0.20 \pm 0.02$.

A few additional experiments were performed at 373 K to detect any temperature dependence of β_1. The measured branching ratio tended to be slightly higher (0.22 ± 0.03), but, with uncertainties being taken into account, it was indistinguishable from the above value. This result allows us to conclude that the branching ratio does not vary significantly in the temperature range considered and that this conclusion is probably valid for the atmospheric temperatures.

TABLE 9: Measured Values of the Branching Ratio β_1 at 298 K

$[CH_3CHO]^a$	$[CH_3OH]^a$	$[CH_3C(O)O_2]_{ini}{}^b$	$[HO_2]_{ini}{}^b$	β_1
1.0	1.0	5.3	3.8	0.22
1.0	2.0	2.8	4.0	0.20
1.0	2.0	3.0	4.6	0.19
1.1	1.6	5.4	5.2	0.18
1.6	1.6	6.7	4.2	0.20
1.1	3.2	3.2	5.0	0.19
1.6	1.6	5.2	3.7	0.19
1.6	1.6	5.05	3.0	0.20
1.6	1.6	5.7	3.8	0.17
1.6	3.2	4.0	4.8	0.19

^{a} Unit: 10^{15} molecule cm^{-3}. ^{b} Unit: 10^{13} molecule cm^{-3}.

Discussion

The first part of the present work was focused on the $HO_2 + CH_3CHO$ reaction, with the aim of determining its kinetic and thermodynamic characteristics. The rate constant k_2 was measured to be 4.4×10^{-14} cm^3 molecule^{-1} s^{-1} at 298 K, with an uncertainty factor of about 2. This value is significantly larger than that estimated by Moortgat et al.,[17] 1×10^{-15} cm^3 molecule^{-1} s^{-1}, but very close to that recently reported by Crawford et al.,[3] $\approx 5 \times 10^{-14}$ cm^3 molecule^{-1} s^{-1}. It is interesting to emphasize that the reaction between HO_2 and HCHO exhibits a similar rate constant, 7.9×10^{-14} cm^3 molecule^{-1} s^{-1} at 298 K.[13] However, the agreement observed between our value and that of Crawford et al.[3] may be fortuitous, since they did not take the reverse reaction into account in the determination of the kinetic parameters. Moreover, they measured the rate constant at temperatures as high as 360 K, whereas, according to the thermochemical parameters determined in this work, the equilibrium should have been completely shifted toward the reactants at that temperature and under their experimental conditions. Thus, they should not have observed any reaction between HO_2 and CH_3CHO. The reasons for this strong disagreement between the work of Crawford et al. at high temperature and the present results are presently unknown.

The similarities between the spectroscopic and kinetic properties of the $CH_3CH(OH)O_2$ and the $CH_2(OH)O_2$ radicals are striking: both spectra exhibit an absorption band of similar shape and centered at 220−230 nm with cross-section values of the same order of magnitude (see Figure 3). Note that the shape of those two radical spectra is close to those generally observed for RO_2 radicals, with smaller absorption cross-sections ($\approx$30%) and a weaker decrease of the absorption band when going toward short wavelengths. In addition, the rate constants of the $CH_3CH(OH)O_2$ radical reactions with itself, HO_2 and CH_3O_2, which were roughly estimated in this work, are those expected for this type of radical.[9] The thermodynamic parameters are also very similar for the reactions of HO_2 with both HCHO and CH_3-CHO. The entropies and enthalpies of reaction are almost the same (in addition, entropies are in agreement with theoretical predictions), and the equilibrium is observed in the same range of temperature for both reactions.[10] Nevertheless, as noted above, the $CH_3CH(OH)O_2$ radical is slightly less stable than the $CH_2(OH)O_2$ radical. All those observations provide confidence in the present results concerning reaction 2.

As emphasized in the Introduction, only two studies[2,3] of the kinetics of reaction 1 between HO_2 and $CH_3C(O)O_2$ have been reported and are in strong disagreement. Therefore, this reaction deserved further studies. The present study has used an experimental setup similar to that used by Moortgat et al.[2] However, the conditions of experiments and of data analysis

were now much better defined than at the time of this previous study.

First, all parameters used in simulations, i.e. absorption cross-sections, rate constants of side reactions, and branching ratios, have been reinvestigated during the past decade and have been reevaluated recently.[4] It results that k_1 was the only important parameter to be adjusted in simulations. The other important parameters, radical cross-sections and rate constants for the self-reactions of CH$_3$C(O)O$_2$ and HO$_2$, are now known with good precision.[4]

Second, the interfering reaction between HO$_2$ and CH$_3$CHO has been investigated in detail in this work, and this has allowed us to select experimental conditions where this reaction was of negligible importance. It is emphasized above that one of the principal reasons for the discrepancy between the two previous studies is likely to result from an inaccurate control of those initial radical concentrations.

The rate constant value, $k_1(298\text{K}) = 1.42 \times 10^{-11}$ cm^3 molecule^{-1} s^{-1}, obtained in this work for reaction 1, confirms the value of Moortgat et al.,[2] though they did not take the reaction between HO$_2$ and CH$_3$CHO (reaction 2) into account. Given the concentration of acetaldehyde they used, around 0.5 Torr,[21] this reaction should have taken place to some extent in their experiments, but not sufficiently to perturb significantly kinetic measurements, since the CH$_3$CH(OH)O$_2$ radical formed in reaction 2 reacts with CH$_3$C(O)O$_2$ at a rate similar to that of HO$_2$. However, the determination of initial radical concentrations was probably perturbed by the occurrence of reaction 2.

It is difficult to understand the high k_1 value reported by Crawford et al.,[3] but it must be noted that (i) the ratios of initial radical concentrations derived from analysis of experimental signals were generally not consistent with precursor concentrations (up to a factor of 3 difference), indicating an insufficiently accurate control of initial radical concentrations; (ii) the reverse reaction -2 was not taken into account in the reaction mechanism and reaction 2 was observed to occur at high temperature (360 K), whereas it should not have taken place, due to the equilibrium shifted toward reactants at that temperature; and (iii) Figure 17 of ref 3 shows that the UV data would be better fitted with the rate constant values reported in this paper and by Moortgat et al.[2] Actually, the rate constant k_1 was essentially derived from the HO$_2$ decay traces observed in the infrared region, which have yielded fairly scattered data. It results that the data reported by Crawford et al.[3] must be regarded with caution.

All previous studies of the branching ratio $\beta_1 = k_{1b}/k_1$,[2,3,5,6] forming ozone, are in fairly poor agreement. Niki et al.[5] first reported an estimated value of $\approx$0.25 for β_1, based on infrared absorption measurements. Moortgat et al.[2] derived, from a study similar to the present one, a higher value, 0.33 at 298 K, independent of temperature in the range 253−368 K. Few details were given on the experimental conditions they used, but it seems that their UV absorption signals were not recorded over sufficiently long time scales and that possible contributions of the remaining peroxy radical absorption have altered the result. In reality, similar high values were found in the present study, with traces recorded over 50 ms, if the branching ratio of the nonterminating channel 14a, regenerating CH$_3$O$_2$ through reactions 12 and 9, was taken equal to that used by Moortgat et al.,[2] i.e. 0.5, whereas a value of 0.9 is now recommended.[4] Note that, in the present study, the best fits of experimental traces were obtained with branching ratio values of 0.6−0.8 for channel 14a. Horie and Moortgat[6] reported a value close to that

of Niki et al.[5] β_1(298K) = 0.27, determined from matrix isolation experiments and FTIR analysis. In contrast to Moortgat et al.,[2] they found a significant temperature dependence, k_{1a}/k_{1b} = 330 exp($-$(1430 K)/T). The present study rather confirms the temperature independent ratio reported by Moortgat et al.[2]

Crawford et al.[3] have recently published a value significantly lower than preceding determinations, $\beta_1 = 0.12$ at 298 K. This value was actually a weighted average between measurements by laser flash photolysis and UV absorption detection (β_1 = 0.16, not far from the present determination) and by determination of the yields of CH$_3$C(O)OH and CH$_3$C(O)OOH and O$_3$, using a smog chamber and FTIR detection: β_1 = 0.10. The temperature dependence of β_1 was reported to be weak.

It must be emphasized, again, that much care was taken in the present work for measuring this branching ratio. The residual absorption was measured at sufficiently long time so that all radicals had disappeared and ozone was the principal absorbing species The small remaining concentration of CH$_3$O$_2$ was taken into account in simulations. Moreover, to make sure that any other absorbing reaction product did not contribute significantly, the spectrum of the residual absorption was recorded from 230 to 280 nm. Both the observed good agreement with the ozone spectrum and the weak scatter of the data (all runs have yielded values included in the 0.17−0.22 range) show the reliability of our measurements.

Conclusion

The kinetic and thermochemical parameters have been characterized for the equilibrated reaction between HO$_2$ and CH$_3$CHO (reactions 2, -2), thus allowing us to quantify the role of these reactions under experimental conditions usually met in the laboratory or in the atmosphere. The parameters have been found to be similar to those already reported for the corresponding reaction of HO$_2$ with HCHO, the adduct CH$_3$-CH(OH)O$_2$ being slightly less stable than its equivalent CH$_2$-(OH)O$_2$. This study was a prerequisite before revisiting the kinetics of reaction 1 between HO$_2$ and CH$_3$C(O)O$_2$, since reaction 2 has been identified as a possible cause of errors in the determination of initial radical concentrations in reaction 1 studies. Thus, reaction 1 was investigated under conditions such that reaction 2 could be ignored, and, consequently, much care could be taken for controlling initial radical concentrations. The results confirm the previous kinetic measurement of Moortgat et al.,[2] despite that the corresponding work was not being performed under the most appropriated conditions.

References and Notes

(1) Beine, H. J.; Jaffe, D. A.; Herring, J. A.; Kelley, J. A.; Krognes, T.; Stordal, F. *J. Atmos. Chem.* **1997**, *27*, 127.

(2) Moortgat, G. K.; Veyret, B.; Lesclaux, R. *Chem. Phys. Lett.* **1989**, *160*, 443.

(3) Crawford, M. A.; Wallington, T. J.; Szente, J. J.; Maricq, M. M.; Francisco, J. S. *J. Phys. Chem. A* **1999**, *103*, 365.

(4) Tyndall, G. S.; Cox, R. A.; Granier, C.; Lesclaux, R.; Moortgat, G. K.; Pilling, M. J.; Ravishankara, A. R.; Wallington, T. J. *J. Geophys. Res.*, in press.

(5) Niki, H.; Maker, P. D.; Savage, C. M.; Breitenbach, L. P. *J. Phys. Chem* **1985**, *89*, 588.

(6) Horie, O.; Moortgat, G. K. *J. Chem. Soc., Faraday Trans.* **1992**, *88*, 3305.

(7) Lightfoot, P. D.; Cox, R. A.; Crowley, J. N.; Destriau, M.; Hayman, G. D., Jenkin, M. E.; Moortgat, G. K.; Zabel, F. *Atmos. Environ., Part A* **1992**, *26*, 1805.

(8) Wallington, T. J.; Dagaut, P.; Kurylo, M. J. *Chem. Rev.* **1992**, *92*, 667.

(9) Lesclaux, R. In *Peroxyl Radicals*; Alfassi Z. B., Ed.; John Wiley & Sons: New York, 1997.

(10) Veyret, B.; Lesclaux, R.; Rayez, M. T.; Rayez, J. C.; Cox, R. A.; Moortgat, G. K. *J. Phys. Chem.* **1989**, *93*, 2368.

(11) Roehl, C. M.; Bauer, D.; Moortgat, G. K. *J. Phys. Chem.* **1996,** *100,* 4038.

(12) Lightfoot, P. D.; Lesclaux, R.; Veyret, B. *J. Phys. Chem.* **1990**, *94*, 700.

(13) Atkinson, R.; Baulch, D. L.; Cox, R. A.; Hampson, R. F., Jr.; Kerr, J. A.; Rossi, M. J.; Troe, J. Evaluated Kinetic and Photochemical Data for Atmospheric Chemistry, Organic Species: Supplement VII. IUPAC Subcommittee on Gas Kinetic Data Evaluation for Atmospheric Chemistry. *J. Phys. Chem. Ref. Data* **1999**, *28***,** 191.

(14) DeMore, W. B.; Sander, S. P.; Golden, D. M.; Hampson, R. F.; Kurylo, M. J.; Howard, C. J.; Ravishankara, A. R.; Kolb, C. E.; Molina, M. J. *NASA JPL Publ.* **1997**, 97−4.

(15) Tyndall, G. S.; Orlando, J. J.; Kegley-Owen, C. S.; Wallington, T. J.; Hurley, M. D. *Int. J. Chem. Kinet.* **1999**, *31*, 776.

(16) Kegley-Owen, C. S.; Tyndall, G. S.; Orlando, J. J.; Fried, A. *Int. J. Chem. Kinet.* **1999**, *31*, 766.

(17) Moortgat, G. K.; Cox, R. A.; Schuster, G.; Burrows, J. P.; Tyndall, G. S. *J. Chem. Soc., Faraday Trans. 2* **1989**, *85*, 809.

(18) Burrows, J. P.; Moortgat, G. K.; Tyndall, G. S.; Cox, R. A.; Jenkin, M. E.; Hayman, G. D.; Veyret, B. *J. Phys. Chem.* **1989**, *93*, 2375.

(19) Dewar, M. J. S.; Zoebisch, E. G.; Healy, E. F.; Stewart, J. J. P. *J. Am. Chem. Soc.* **1985**, *107*, 3902.

(20) Atkinson, R.; Baulch, D. L.; Cox, R. A.; Hampson, R. F., Jr.; Kerr, J. A.; Rossi, M. J.; Troe, J. Evaluated Kinetic, Photochemical and Heterogeneous Data for Atmospheric Chemistry: Supplement V. IUPAC Subcommittee on Gas Kinetic Data Evaluation for Atmospheric Chemistry. *J. Phys. Chem. Ref. Data* **1997**, *26*, 521.

(21) Moortgat, G. K.; Veyret, B. Personal communication.

(22) Villenave, E.; Lesclaux, R.; Seefeld, S.; Stockwell, W. R., *J. Geophys. Res.* **1998**, *103*, D19, 25273.

(23) Villenave, E.; Lesclaux, R, *J. Phys. Chem*. **1996**, *100*, 14372.